FAILURE ANALYSIS OF THICK LAMINATES UNDER OUT-OF-PLANE SHEAR

Jia Liyong[1,*], Jia Yuming[1], Li Miao [1], Yu Long[2], Zhang Kuangyi[2], J. P. Dear[2]

[1] First Aircraft Institute of AVIC, Xi'an 710089, China

[2] Department of Mechanical Engineering, Imperial College London, South Kensington Campus, London SW7 2AZ, UK

Keywords: Thick laminates, Multi-scale modelling , Cohesive zone model, Shear nonlinearity, VUMAT

ABSTRACT

A multi-scale model based on sub-laminate homogenization and decomposition of sub-laminate stress and strain is presented to analyse thick composite structural failure, and in which the shear nonlinearity is considered. The thick-sectioned laminates are modelled at a sub-laminate level whilst the structural failure is predicted at a ply level. In addition, an improved cohesive zone model which considers the resistance of inter-laminar compressive stress is used to predict the inter-laminar delamination. Two user-defined FORTRAN subroutines (VUMAT) have been written for ABAQUS/EXPLICIT solver and is used to model the shear nonlinearity , intra-laminar and inter-laminar failure. The modelling has been employed to predict the failure processes for Iosipescu shear test specimens. The results show that both the failure mode and the load-displacement trace for finite element simulations match well the experimental findings. This demonstrates the validity of the multi-scale nonlinear three-dimensional model for thick laminates and the compressive resistant cohesive zone model for inter-laminar delamination. These simulations are validated by experiments using Digital Image Correlation (DIC).

1 INTRODUCTION

For thick composite laminates, the span to thickness ratio is relatively small and out-of-plane effects cannot be ignored, hence classical sheet or shell theory is not suitable for such problems. Therefore, three-dimensional modelling and three-dimensional failure criteria should be employed. Most commercial finite element softwares for composite structure analysis are based on the classical two-dimensional laminate theory or three-dimensional ply-by-ply modelling [1,2,3]. For composite laminates with hundreds of layers, a three-dimensional ply-by-ply FEA model would be too time-consuming in calculation and not suitable for engineering analysis.

For three-dimensional failure criterion, there are severall solutions based on meso-mechanics [4, 5, 6] and macro-mechanics [7, 8, 9, 10] in The Second World-Wide Failure Exercise (WWFE-II). In these analyses, most are based on a ply-by-ply approach except for Bogetti's multi-scale theory [10]. By using sub-laminate homogenization and decomposition of stresses and strains, Bogetti's multi-scale theory could effectively reduce the number of elements in the thickness direction of a laminate and it is quite suitable for modelling thick composite laminates[11]. Based on this approach, several kinds of user subroutines are developed to solve thick laminates problems [12]. In these subroutines, the tangent stiffness is used to calculate the nonlinear shear stresses,a very small load increment is required to calculate the stresses but the tangent stiffness method is not self-correcting and numerical errors can be accumulated. Besides, when using the above subroutines, a database file which contains material and layup information will be read repeatedly from local hard disk of a computer or server [13,14]. Reading data in this way is inefficient and would cause errors when multiple processors are used for parallel computing.

* Corresponding author. Tel.: +86-029-86832604

E-mail address: taishanbuzuo@163.com

Specially, for prediction of inter-laminar delamination, cohesive zone model is an effective and widely used approach. Hower, most cohesive zone models ignore the influence of inter-laminar compressive stress in predicting damage initiation[15,16].

This paper presents an improvement of the above multi-scale approach and traditional cohesive zone model. Chou's equivalent theory [17] is employed to calculate the equivalent elastic constants of sub-laminates and the self-correcting secant stiffness is used to describe the shear non-linearity. An improved cohesive zone model which considers the resistance of inter-laminar compressive stress is used to predict the inter-laminar delamination. Two user-defined material subroutines VUMAT is written for ABAQUS/EXPLICIT solver. One is used for predicting intra-laminar failure and the other is used for predicting the inter-laminar failure.

2 MULTI-SCALE MODELLING OF STRESS-STRAIN BEHAVIOUR

2.1 The multi-scale approach

In this multi-scale approach, a thick laminate is divided into several sub-laminates in the thickness direction. For each sub-laminate, there are a number of plies in it. For each sub-laminate, the equivalent stiffness should be calculated firstly. After this calculation, the equivalent stiffness is used to calculate the general response of the structure, like global sub-laminate level displacements, stresses and strains. Then, the local ply level stresses and strains in the material coordinate system are obtained through coordinate transformation and decomposition of sub-laminate level stresses and strains. Final step is to predict the damage status and the corresponding stiffness reduction. This procedure is shown in Figure 1(a). In order to compare the difference between the multi-scale modelling and the traditional ply-by-ply modelling, the procedure of ply-by-ply analysis is also supplied (see Figure 1(b)).

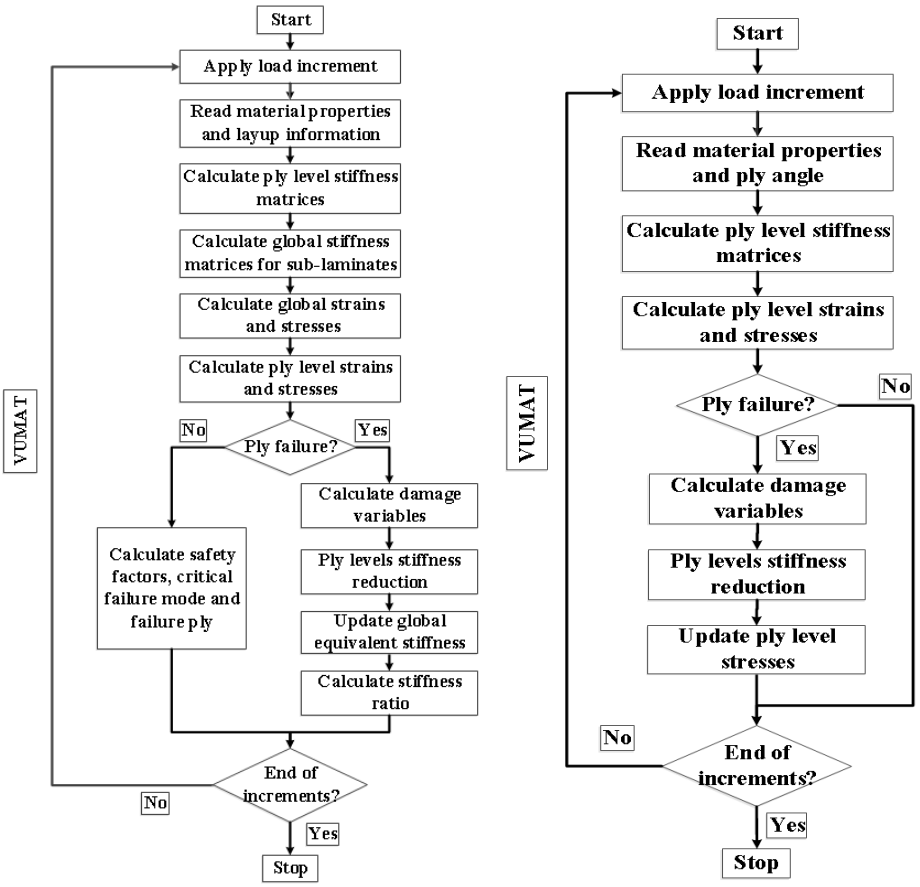

(a) Multi-scale modelling (b) Ply-by-ply modelling

Figure 1: Procedure for multi-scale and ply-by-ply modelling.

2.2 3D equivalent stiffness

According to Chou's 3D equivalent theory [17], a sub-laminate with a number of plies could be equivalent to a monoclinic or orthotropic material, the equivalent stiffness matrix is shown as follows:

$$\left[\bar{C}_{ij}^{*}\right]=\begin{bmatrix} \bar{C}_{11}^{*} & \bar{C}_{12}^{*} & \bar{C}_{13}^{*} & 0 & 0 & \bar{C}_{16}^{*} \\ & \bar{C}_{22}^{*} & \bar{C}_{23}^{*} & 0 & 0 & \bar{C}_{26}^{*} \\ & & \bar{C}_{33}^{*} & 0 & 0 & \bar{C}_{36}^{*} \\ & & & \bar{C}_{44}^{*} & \bar{C}_{45}^{*} & 0 \\ & sym & & & \bar{C}_{55}^{*} & 0 \\ & & & & & \bar{C}_{66}^{*} \end{bmatrix} \tag{1}$$

where the barred notation "¯"represents the stiffness coefficient in the global coordinate system of the laminate and the star "*" signifies an equivalent value. The stress-strain constitutive relationship for the sub-laminate is described as:

$$[\bar{\sigma}^{*}]=[\bar{C}_{\mathrm{ij}}^{*}][\bar{\varepsilon}^{*}] \tag{2}$$

where $\left[\bar{\sigma}^{*}\right]$ and $\left[\bar{\varepsilon}^{*}\right]$ are the global equivalent stresses and strains.

The coefficients of the sub-laminate stiffness matrix, $\bar{C}_{ij}^{*}$, are defined in Equations 3 to 6:

$$\bar{C}_{ij}^{*}=\sum_{k=1}^{n}V^{k}\left[\bar{C}_{ij}^{k}-\frac{\bar{C}_{i3}^{k}\bar{C}_{3j}^{k}}{\bar{C}_{33}^{k}}+\frac{\bar{C}_{i3}^{k}\sum_{l=1}^{n}\frac{V^{l}\bar{C}_{3j}^{k}}{\bar{C}_{33}^{k}}}{\bar{C}_{33}^{k}\sum_{l=1}^{n}\frac{V^{l}}{\bar{C}_{33}^{k}}}\right]\quad(i,j=1,2,3,6) \tag{3}$$

$$\bar{C}_{ij}^{*}=\bar{C}_{ji}^{*}=0\quad(i=1,2,3,6;\ j=4,5) \tag{4}$$

$$\bar{C}_{ij}^{*}=\frac{\sum_{k=1}^{n}\frac{V^{k}}{\Delta_{k}}\bar{C}_{ij}^{k}}{\sum_{k=1}^{n}\sum_{l}^{n}\frac{V^{k}V^{l}}{\Delta_{k}\Delta_{l}}\left(\bar{C}_{44}^{k}\bar{C}_{55}^{l}-\bar{C}_{45}^{k}\bar{C}_{54}^{l}\right)}\quad(i,j=4,5) \tag{5}$$

$$\Delta_{k}=\bar{C}_{44}^{k}\bar{C}_{55}^{k}-\bar{C}_{45}^{k}\bar{C}_{54}^{k} \tag{6}$$

where k refers to the k^{th} ply of the sub-laminate, n represents the number of plies in the sub-laminate, V^{k} is the ratio of the original thickness of the k^{th} ply to the original total thickness of the entire sub-laminate and $\bar{C}_{ij}^{k}$ represents the stiffness coefficient of the k^{th} ply in a sub-laminate in the global coordinate system. This is obtained from coordinate transformation of stiffness matrix in local material coordinate system [18].

2.3 Stress and strain decomposition

With the global equivalent stiffness, the general response of the entire structure, like global stresses $\left[\bar{\sigma}^{*}\right]$ and strains $\left[\bar{\varepsilon}^{*}\right]$ can be easily obtained. However, all these values are in sub-laminate level. In order to decompose the ply level stresses and strains, the following assumptions should be introduced [10]:

$$\bar{\varepsilon}_{i}^{k}=\bar{\varepsilon}_{i}^{*}\quad(i=1,2,6;k=1,2,\cdots,n) \tag{7}$$

$$\bar{\sigma}_{i}^{k}=\bar{\sigma}_{i}^{*}\quad(i=3,4,5;k=1,2,\cdots,n) \tag{8}$$

where $\bar{\sigma}_i^k$ and $\bar{\varepsilon}_i^k$ are the stress and strain components for the k^{th} ply in global coordinate system, and $\bar{\sigma}_i^*, \bar{\varepsilon}_i^*$ refer to the stress and strain components for the sub-laminate in global coordinate system. With the above assumptions, all the remained ply level stress and strain components could be obtained from Equations 9 and 10:

$$\begin{bmatrix} \bar{\varepsilon}_3^k \\ \bar{\varepsilon}_4^k \\ \bar{\varepsilon}_5^k \end{bmatrix} = \begin{bmatrix} \bar{C}_{33}^k & \bar{C}_{34}^k & \bar{C}_{35}^k \\ \bar{C}_{43}^k & \bar{C}_{44}^k & \bar{C}_{45}^k \\ \bar{C}_{53}^k & \bar{C}_{54}^k & \bar{C}_{55}^k \end{bmatrix}^{-1} \left[\begin{bmatrix} \bar{\sigma}_3^k \\ \bar{\sigma}_4^k \\ \bar{\sigma}_5^k \end{bmatrix} - \begin{bmatrix} \bar{C}_{31}^k & \bar{C}_{32}^k & \bar{C}_{36}^k \\ \bar{C}_{41}^k & \bar{C}_{42}^k & \bar{C}_{46}^k \\ \bar{C}_{51}^k & \bar{C}_{52}^k & \bar{C}_{56}^k \end{bmatrix} \begin{bmatrix} \bar{\varepsilon}_1^k \\ \bar{\varepsilon}_2^k \\ \bar{\varepsilon}_6^k \end{bmatrix} \right] \quad (k = 1,2,\cdots,n) \tag{9}$$

$$\begin{bmatrix} \bar{\sigma}_1^k \\ \bar{\sigma}_2^k \\ \bar{\sigma}_6^k \end{bmatrix} = \begin{bmatrix} \bar{C}_{11}^k & \bar{C}_{12}^k & \bar{C}_{13}^k & \bar{C}_{14}^k & \bar{C}_{15}^k & \bar{C}_{16}^k \\ \bar{C}_{21}^k & \bar{C}_{22}^k & \bar{C}_{23}^k & \bar{C}_{24}^k & \bar{C}_{25}^k & \bar{C}_{26}^k \\ \bar{C}_{61}^k & \bar{C}_{62}^k & \bar{C}_{63}^k & \bar{C}_{64}^k & \bar{C}_{65}^k & \bar{C}_{66}^k \end{bmatrix} \begin{bmatrix} \bar{\varepsilon}_1^k \\ \bar{\varepsilon}_2^k \\ \bar{\varepsilon}_3^k \\ \bar{\varepsilon}_4^k \\ \bar{\varepsilon}_5^k \\ \bar{\varepsilon}_6^k \end{bmatrix} \quad (k = 1,2,\cdots,n) \tag{10}$$

Before predicting the failure status of each ply, the ply level stresses and strains in global coordinate system have to be transformed to local material coordinate system.

2.4 Non-linear shear constitutive response

The non-linear stress-strain relationship between τ_{13} and γ_{13} is defined as[19]:

$$\tau_{13} = \frac{G_{13}^0 \gamma_{13}}{\left(1 + \left(\frac{G_{13}^0 \gamma_{13}}{S_{13}}\right)^{\text{n}}\right)^{\frac{1}{n}}} \tag{11}$$

The secant modulus G_{13}^s could be obtained by the following equation [19]:

$$G_{13}^s = \frac{\tau_{13}}{\gamma_{13}} = \frac{G_{13}^0}{\left(1 + \left(\frac{G_{13}^0 \gamma_{13}}{S_{13}}\right)^{\text{n}}\right)^{\frac{1}{n}}} \tag{12}$$

Where G_{13}^0 is the initial shear modulus, S_{13} refers to the shear strength and *n* is the shape factor of the nonlinear stress-strain curve. The parameter *n* is determined by fitting to experimental data as shown in Figure 2.

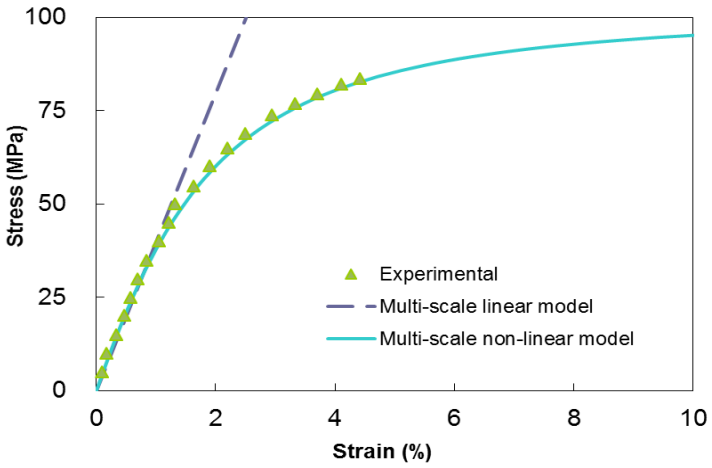

Figure 2: Non-linear stress-strain relationship and the effect of shape factor.

3. PROGRESSIVE FAILURE MODELLING

3.1 Intra-laminar failure model

For in-plane fibre tensile and compressive failure, the maximum-stress criterion is used [8,20,21, 22]：

$$f_{ft} = \frac{\sigma_{11}}{X_T} \quad (\sigma_{11} \geq 0) \tag{13}$$

$$f_{fc} = -\frac{\sigma_{11}}{X_C} \quad (\sigma_{11} < 0) \tag{14}$$

where X_T and X_C are the longitudinal tensile and compressive strength.

For matrix failure, the Hashin criterion is introduced[7].

$$\left(\frac{\sigma_{22}+\sigma_{33}}{Y_T}\right)^2 + \frac{\sigma_{23}^2 - \sigma_{22}\sigma_{33}}{S_T^2} + \frac{\sigma_{12}^2+\sigma_{13}^2}{S_L^2} \geq 1 \quad (\sigma_{22}+\sigma_{33} \geq 0) \tag{15}$$

$$\left[\left(\frac{Y_C}{2S_T}\right)^2 - 1\right]\frac{\sigma_{22}+\sigma_{33}}{Y_C} + \left(\frac{\sigma_{22}+\sigma_{33}}{2S_T}\right)^2 + \frac{\sigma_{23}^2 - \sigma_{22}\sigma_{33}}{(S_T)^2} + \frac{\sigma_{12}^2+\sigma_{13}^2}{(S_L)^2} \geq 1 \quad (\sigma_{22}+\sigma_{33} < 0) \tag{16}$$

where Y_T and Y_C are the transverse tensile and compressive strength, S_L and S_T are the longitudinal and transverse (to the fibres) shear strengths,

For fibre failure, the damage variable d_f is given by:

$$d_f = 1-(1-d_{ft})(1-d_{fc}) \tag{17}$$

where

$$d_{ft}(\varepsilon_{11}) = \frac{\varepsilon_{f,1}^t}{\varepsilon_{f,1}^t - \varepsilon_{0,1}^t}\left(1 - \frac{\varepsilon_{0,1}^t}{\varepsilon_{11}}\right) \tag{18}$$

$$d_{fc}(\varepsilon_{11}) = \frac{\varepsilon_{f,1}^c}{\varepsilon_{f,1}^c - \varepsilon_{0,1}^c}\left(1 - \frac{\varepsilon_{0,1}^c}{\varepsilon_{11}}\right) \quad . \tag{19}$$

The index t and c refer to the tensile and compressive behaviours, respectively, $\varepsilon_{0,1}^t$ and $\varepsilon_{0,1}^c$ correspond to the strain in tension and compression at failure initiation point, $\varepsilon_{f,1}^t$ and $\varepsilon_{f,1}^c$ correspond to the maximum strain in tension and compression when the damage variables are equal to one. The maximum failure strain $\varepsilon_{f,1}^t$ and $\varepsilon_{f,1}^c$ can be obtained by:

$$\varepsilon_{f,1}^{t} = \frac{2G_{IC}^{t}}{X_T L} \tag{20}$$

$$\varepsilon_{f,1}^{c} = \frac{2G_{IC}^{c}}{X_C L} \tag{21}$$

where X_T and X_C are the tensile and compressive strength in fibre direction, G_{IC}^{t} and G_{IC}^{c} are the intra-laminar fracture toughness in fibre tension and compression and L is the characteristic length of an element.

The stress–strain behaviour in fibre tension and compression before and after damage occurs is depicted in Figure 3.

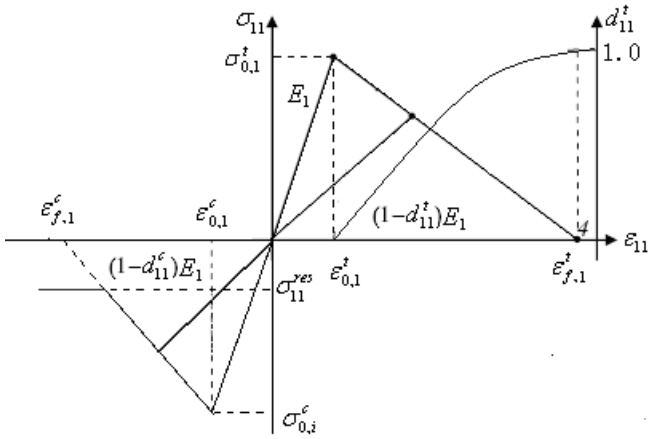

Figure 3 : Material behaviour in the longitudinal direction.

The total damage for fibre and matrix are defined as:

$$d_f = 1-(1-d_{ft})(1-d_{fc}) \tag{22}$$

$$d_m = 1-(1-d_{mt})(1-d_{mc}) \tag{23}$$

When damage occurs in the k^{th} ply, the stiffness matrix for this damage ply is updated by

$$\mathbf{C}_d^k = \begin{bmatrix} (1-d_f)C_{11}^0 & (1-d_f)(1-d_m)C_{12}^0 & (1-d_f)C_{13}^0 & 0 & 0 & 0 \\ (1-d_f)(1-d_m)C_{12}^0 & (1-d_m)C_{22}^0 & (1-d_m)C_{23}^0 & 0 & 0 & 0 \\ (1-d_f)C_{13}^0 & (1-d_m)C_{23}^0 & C_{33}^0 & 0 & 0 & 0 \\ 0 & 0 & 0 & (1-d_m)C_{44}^0 & 0 & 0 \\ 0 & 0 & 0 & 0 & (1-d_f)C_{55}^0 & 0 \\ 0 & 0 & 0 & 0 & 0 & (1-d_f)(1-d_m)C_{66}^0 \end{bmatrix} \tag{24}$$

where C_{ij}^0 is the undamaged stiffness coefficient in the local material coordinate system.

After the damaged stiffness matrix for the k^{th} ply in local material coordinate system C_d^k is obtained, it should be transformed from the local material coordinate system to the global coordinate system in order to get the global damaged stiffness matrix, $\bar{C}_d^k$, and then, Equations 5 to 8 are employed again to calculate the global damaged equivalent stiffness matrix for one sub-laminate, $\bar{C}_d^*$.

For thick laminated structures, it is hard to monitor the damage variables for each ply, which will waste a large amount of computation time and storage space. In order to solve this problem, stiffness ratio for sub-laminate is introduced [10-12], it is shown as follows:

$$R_{ij} = \frac{\bar{C}_{ij}^{c,*}}{\bar{C}_{ij}^{0,*}} \quad (i, j = 1,6) \tag{25}$$

where R_{ij} represents the stiffness ratio, $\bar{C}_{ij}^{0,*}$ is the equivalent undamaged stiffness coefficient in global coordinate system at the beginning of loading, and $\bar{C}_{ij}^{c,*}$ is the current equivalent damaged or discounted stiffness coefficient in global coordinate system. The initial valve of each stiffness ratio is 1.0. At the beginning of each load increment, all the stiffness ratios are used to update the current stiffness coefficients, whilst, at the end of each load increment, the up-to-date stiffness radios will be calculated and saved according to the current damage status.

3.3Modified cohesive zone model

A modified Quadratic nominal stress criterion is introduced to predict delamination initiation, in which the influence of compressive normal stress is considered:

$$f_{3t} = \left[\frac{\sigma_n}{N_{\max}}\right]^2 + \left[\frac{\sigma_t}{T_{\max}}\right]^2 + \left[\frac{\sigma_s}{S_{\max}}\right]^2 \qquad (\sigma_n \geq 0) \tag{26}$$

$$f_{3c} = \left[\frac{\sigma_t}{T_{\max} - \mu_t \sigma_n}\right]^2 + \left[\frac{\sigma_s}{S_{\max} - \mu_s \sigma_n}\right]^2 \qquad (\sigma_n < 0) \tag{27}$$

Where $\sigma_n, \sigma_s, \sigma_t$ represent the normal and the two shear tractions , $N_{\max}, T_{\max}, S_{\max}$ represent the peak values of the nominal stress when the deformation is either purely normal to the interface or purely in the first or the second shear direction, μ_t and μ_s are friction coefficients in the first or the second shear direction.

The Benzeggagh-Kenane fracture criterion is used to define the mixed mode damage evolution:

$$G_C = G_{IC} + (G_{IIC} - G_{IC})[(G_{II} + G_{III}) / (G_I + G_{II} + G_{III})]^{\eta} \tag{28}$$

Where G_{IC}, G_{IIC} refer to the critical fracture energies required to cause failure in the normal and the first shear directions, η is a Numerical factor .

4 COMPARISON OF SIMULATION WITH EXPERIMENTAL RESULTS

4.1 Validation of multi-scale approach

Six virtual composite laminates ($[0_8]$,$[0/90/90/0]_s$,$[0/45/-45/0]_s$,$[0_{32}]$,$[0/90/90/0]_{4s}$ and $[0/45/-45/0]_{4s}$) measuring $20\times10\text{mm}^2$ were used to evaluate the performance of the multi-scale approach. The laminates were continuously loaded in the fibre direction under displacement control. The material system of the specimen is CCF300/5228A with mechanical properties given in Table 1, and the thickness for a single ply is 0.125mm.

E_1 (MPa)	E_2 (MPa)	E_3 (MPa)	υ_{12}	υ_{13}	υ_{23}	G_{12} (MPa)	G_{13} (MPa)	G_{23} (MPa)
138000	9040	9040	0.307	0.307	0.35	4500	4500	3476
X_T (MPa)	X_C (MPa)	Y_T (MPa)	Y_C (MPa)	S_L (MPa)	S_T (MPa)	n	G_{12}^0 (MPa)	G_{13}^0 (MPa)
1696	1188	71.4	202	102	90	1.3	4500	4500

Table 1: Mechanical property of uni-axial laminates.

For comparison purpose, the load-displacement responses for the composite panel with multi-scale modelling and traditional ply-by-ply modelling are represented on a single graph. All the computation is implemented by using the same number of CPUs and under the same hardware conditions, the loading velocity in each FEA model is also the same. Figure 4 compares the structural response obtained by using the two different modelling approaches for laminate with 6 kinds of stacking sequence. Table 2 compares the accuracy and computing efficiency for the two different modelling methods for these composite laminates.

From Figure 4, the load versus displacement trace for the current multi-scale modelling and traditional ply-by-ply modelling are similar. Table 2 also gives the first peak load and the maximum load obtained from the two methods which are also similar. This demonstrates that the accuracy of

multi-scale modelling is acceptable. Moreover, the stable time increment for the multi-scale modelling is much larger than that for ply-by-ply modelling. With such a larger stable time increment and relatively fewer finite elements, the current multi-scale modelling is much more efficient in calculation than that of the traditional ply-by-ply modelling.

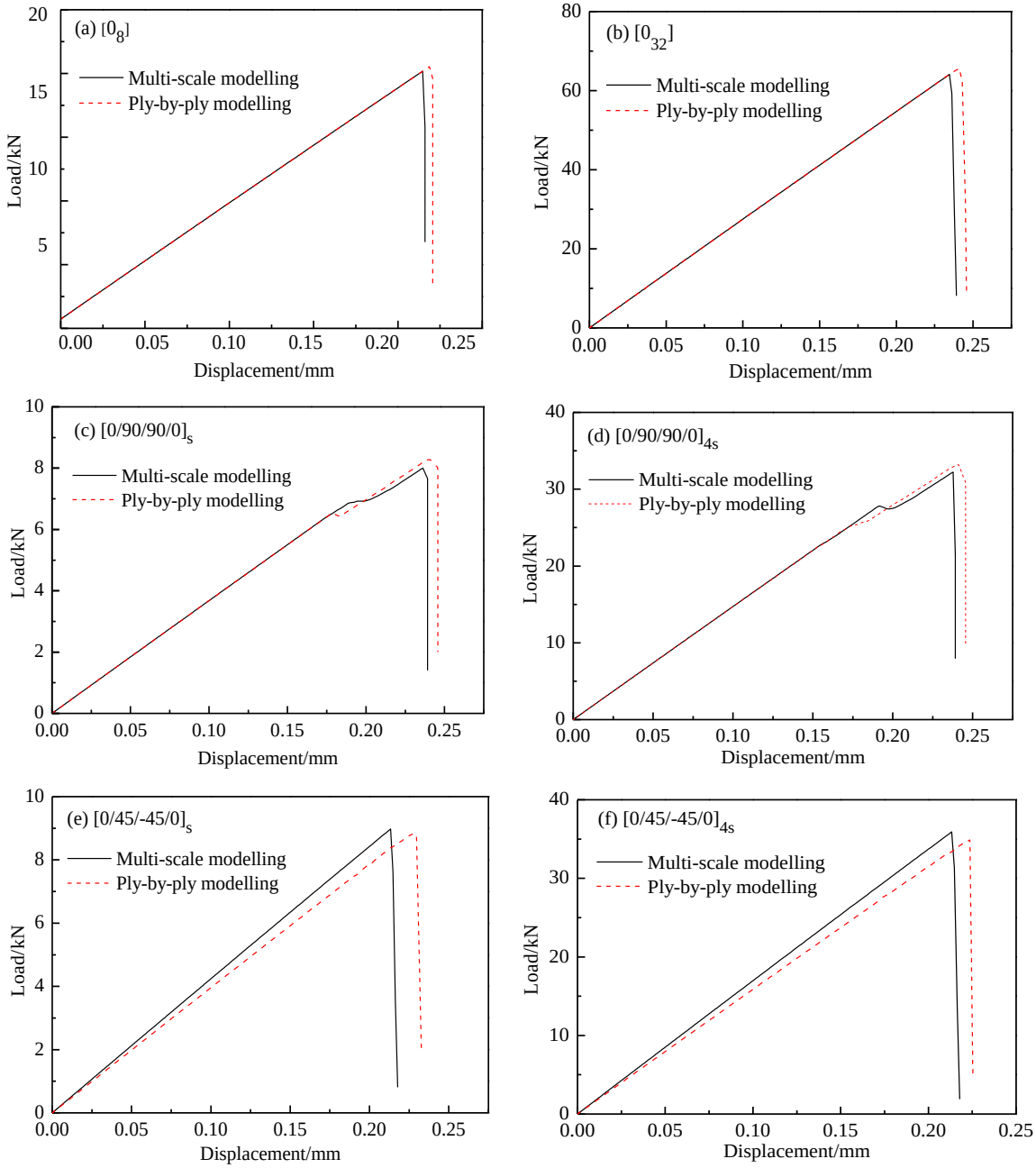

Figure 4: Comparison of load-displacement curves for uni-axial traction models of CCF300/5228A laminates with different layup sequences

Layup information	Modelling type	First peak load/N	Maximum load/N	Stable time increment
$[0_8]$	Multi-scale		16113.5	1.375e-07
	Ply-by-ply		16409.5	4.806e-08
$[0_{32}]$	Multi-scale		64103.4	1.215e-07
	Ply-by-ply		65528.9	4.806e-08
$[0/90/90/0]_s$	Multi-scale	6687.5	8002.9	1.847e-07
	Ply-by-ply	6303.6	8285.0	4.806e-08
$[0/90/90/0]_{4s}$	Multi-scale	26776.0	32219.9	2.078e-07
	Ply-by-ply	24574.4	33208.0	4.806e-08
$[0/45/-45/0]_s$	Multi-scale		8977.9	1.375e-07
	Ply-by-ply		8817.5	3.779e-08
$[0/45/-45/0]_{4s}$	Multi-scale		35926.0	1.917e0-7
	Ply-by-ply		34913.3	3.779e-08

Table 2: Comparison of accuracy and computing efficiency for different CCF300/5228A uni-axial traction models with two kinds of analysis methods

4.2 Out-of-plane shear test and simulation for thick laminates

Iosipescu shear test (G13 shear test) is designed according to ASTM D5379 standard [23].The test fixture is shown in Figure 5(a). For the G13 shear test specimen, the fibres are along the longitudinal direction of the specimen (see Figure 5 (b)).

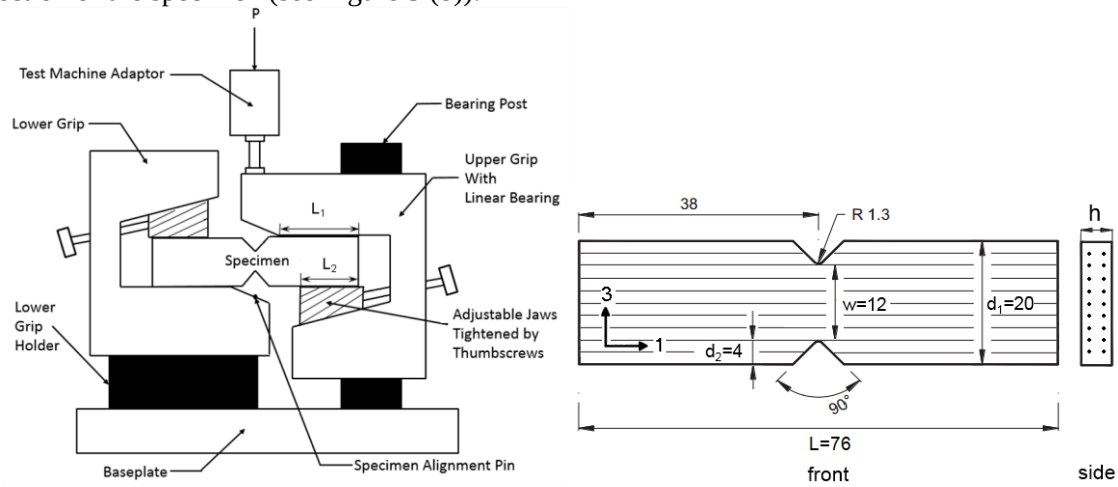

(a)Fixture schematic for Iosipescu shear test (b) Dimensions for G13 shear test specimen

Figure 5: Specimen dimensions and test fixture schematic for Iosipescu shear test (dimensions in mm).

For each specimen with 160 plies, the thickness, d_1, is 20 mm and the entire laminate is divided into 20 sub-laminates through the thickness direction, each sub-laminate is modelled with C3D8R elements, specially, for the G13 shear test, 5 layers of cohesive elements (COH3D8) are used to model the failure of delamination [24]. The dimensions of the specimens are given in Figures 5(b).

Table 1 gives the mechanical properties of the composite laminate from the material supplier data sheet and Table 3 gives the inter-laminar stiffness, strength and fracture toughness of the cohesive zone model, which are used in the modelling. The G13 shear test results are shown in Figure 6 for when the fibres are along the longitudinal direction. The shear test specimens were continuously loaded under displacement control and the full field strain fields were measured through 3D Digital Image Correlation (DIC). The G13 shear tests are firstly presented for specimens of out of plane height, h=5 mm.

E (MPa)	G (MPa)	N_0 (MPa)	S_0 (MPa)	T_0 (MPa)	G_{IC} (N/mm)	G_{IIC} (N/mm)	G_{IIIC} (N/mm)
9000	4500	71.4	102	102	0.75	1.5	1.5

Table 3. Inter-laminar stiffness, strength and fracture toughness of composite laminate for Iosipescu shear tests.

Figure 6 shows experimental load-displacement curve (Figure 6(a)), comparison with FEA (Figure 6(b)) , strain fields from DIC (Figure 6 (c)) and FEA (Figure 6(d) and Figure 6(e)).

Four specimens (Experiment 1,Experiment 2, Experiment 3, and Experiment 4) were tested to confirm the reproducibly of the experiments and the results are shown in Figure 6(a). Figure 6(b) compares the simulated load-displacement curves with the experimental data for Experiment 3. Three numerical approach have been used to predict the structural response of the specimen: the linear multi-scale model, the non-linear multi-scale model(non-linear model 1) and non-linear multi-scale model with modified cohesive zone model (non-linear model 2).

The load-displacement curve obtained from the non-linear multi-scale model fits better than the linear model, especially the modified non-linear model. For the first peak load, the error between non-linear multi-scale model and the average experimental results is less than 1%, whilst the error of linear multi-scale model is larger than 5%. For the maximum load, the error of non-linear multi-scale model is less than 5%, whilst the error for linear multi-scale model is larger than 10 %. It is clear that, for G13 shear test, the non-linear effect of material on structural response is significant and cannot be ignored. The improved non-linear model with modified cohesive zone model is more consistent with the experimental results.

Figures 6 (c),6 (d) and 6 (e) show the comparison of failure mode and maximum principal strain from DIC and non-linear FEA for the G13 shear test (h=5mm). It can be seen that the predicted onset of failure and the position of strain concentration are in good agreement with experimental results from DIC. But there is notable difference for the position and value of the maximum principal strain in the strain plots. The reason for this difference is that, when damage is initiated in the FEA model, the corresponding elements will be deleted in the FEA model so as to form the cracks, so the maximum principal strain becomes zero. However, for the DIC strain plots, when a crack appears and the size of the crack is small, the strain value around the tip of the crack is very large (this is the area in red in Figure 6(c)).

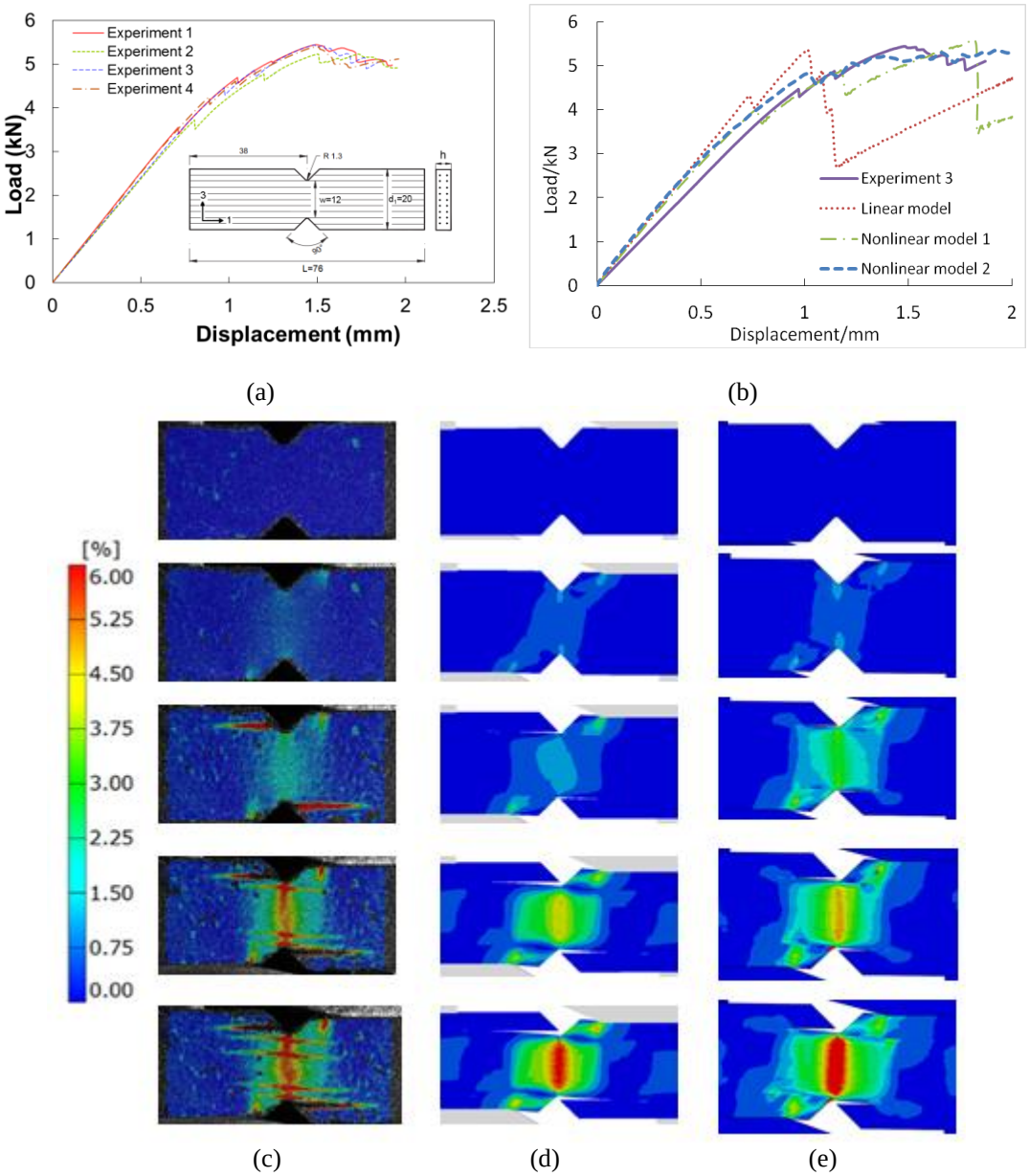

Figure 6. Comparison of experimental and simulated results for G13 shear test (h=5mm): (a) Experimental load versus displacement trace; (b) Comparison of experimental and simulated load-displacement traces; (c) Failure mode and maximum principal strain from DIC; (d) Failure mode and maximum principal strain from non-linear model 1; (e) Failure mode and maximum principal strain from non-linear model 2.

To demonstrate the versatility of the three-dimensional multi-scale modelling, experiments and FEA analysis for G13 (h=3 mm) were performed. The linear multi-scale model and two non-linear multi-scale models are used to predict the structural response of the specimen. As shown in Figure 7, the comparison between experimental and simulated load-displacement curves confirms that, for G13 shear test, the non-linear multi-scale approach with modified cohesive zone model has a much higher accuracy than the linear model.

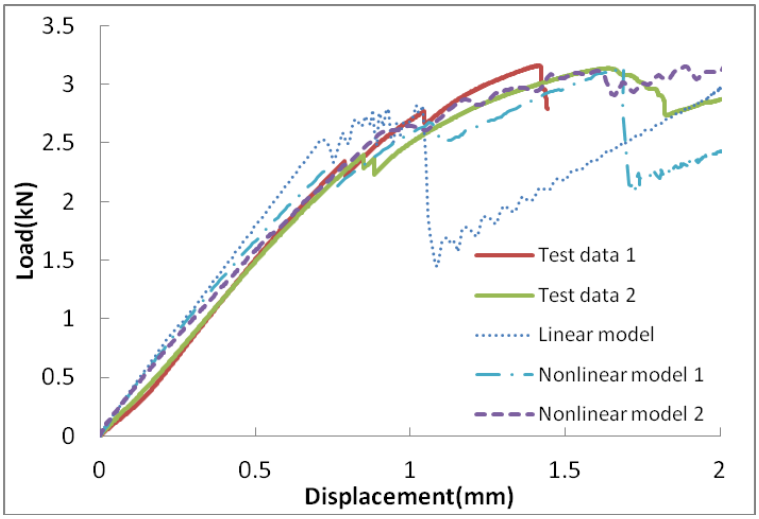

Figure7. Comparison of experimental and simulated load-displacement traces (h=5mm)

5 CONCLUSIONS

A non-linear multi-scale methodology based on sub-laminate homogenization and decomposition of sub-laminate stresses and strains has been presented for solving progressive failure problems in thick composite laminate. A modified cohesive zone model which considers the resistance of inter-laminar compressive stress is used to predict the inter-laminar delamination. The model effectively predicts the failure mode, peak load and crack propagation path with good accuracy. The comparison between linear multi-scale model and two non-linear multi-scale model on predicting the structural response of G13 shear test shows that the non-linear effect of material on structural response is significant and the non-linear model is much more accurate than traditional linear model.

REFERENCES

[1] DS.SIMULIA.ABAQUS User Manual. Version 6.10, ABAQUS Inc., Providence, RI, USA, 2010.

[2] Hallquist J O. LS-DYNA theory manual [J]. Livermore software Technology Corporation, 2006, 3.

[3] Dytran MSC. Theory manual [J]. Wydawnictwo MSC, 2013.

[4] Zhou Y X, Huang Z M. A bridging model prediction of the ultimate strength of composite laminates subjected to triaxial loads [J]. Journal of Composite Materials, 2012: 46: 2343–2378.

[5] Carrere N, Laurin F, Maire J F. Micromechanical-based hybrid mesoscopic 3D approach for non-linear progressive failure analysis of Failure models and criteria for frp under in-plane or three-dimensional stress states including shear non-linearity. composite structures[J]. Journal of Composite Materials, 2012, 46(19-20): 2389-2415.

[6] Nelson E E, Hansen A C, Mayes J S. Failure analysis of composite laminates subjected to hydrostatic stresses: A multicontinuum approach[J]. Journal of Composite Materials, 2012, 46(19-20): 2461-2483.

[7] Hashin Z. Failure criteria for unidirectional fiber composites[J]. Journal of applied mechanics, 1980, 47(2): 329-334.

[8] Pinho S T, Darvizeh R, Robinson P, et al. Material and structural response of polymer-matrix fibre-reinforced composites[J]. Journal of Composite Materials, 2012, 46(19-20): 2313-2341.

[9] Deuschle H M, Puck A. Application of the Puck failure theory for fibre-reinforced composites under three-dimensional stress: Comparison with experimental results[J]. Journal of Composite Materials, 2013, 47(6-7): 827-846.

[10] Bogetti T A, Staniszewski J, Burns B P, et al. Predicting the nonlinear response and progressive failure of composite laminates under tri-axial loading[J]. Journal of Composite Materials, 2012,46: 2443–2459.

[11] Bogetti, T A, Hoppel, C P R, Drysdale W H. Three-Dimensional Effective Property and Strength Prediction of Thick Laminated Composite Media[R]. U.S. Army Research Laboratory: Aberdeen Proving Ground, MD, October 1995.

[12] Staniszewski J M, Bogetti T A, Keefe M. An Improved Design Methodology for Modeling Thick-Section Composite Structures Using a Multiscale Approach[R]. U.S. Army Research Laboratory: Aberdeen Proving Ground, MD, 2012.

[13] Bogetti, T. A.; Hoppel, C.P.R.; Burns, B. P. LAMPAT: A Software Tool for Analyzing and Designing Thick Laminated Composite Structures; Technical Report 890; U.S. Army Research Laboratory: Aberdeen Proving Ground, MD, September 1995.

[14] Staniszewski J M, Bogetti T A. LAMPAT and LAMPATNL User's Manual[R]. ARMY RESEARCH LAB ABERDEEN PROVING GROUND MD WEAPONS AND MATERIALS RESEARCH DIRECTORATE, 2012.

[15]Camanho PP, et al. Numerical simulation of mixed-mode progressive delamination in the composite materials[J]. J Compos Mater 2003; 37:1415-1438.

[16]Alfano G, Crisfield MA. Finite element interface models for the delamination analysis of laminated composites: mechanics and computational issues[J]. Int J Numer Meth Eng 2001; 50: 1701-1736.

[17] Chou P C, Carleone J, Hsu C M. Elastic constants of layered media[J].Journal of Composite Material,1972,6(1):80-93

[18] JIANG Yongqiu,LU Fengsheng,GU Zhijian. Composite Material Mechanics[M].Xi′an: Xi′an Jiaotong University, October 1993

[19] Richard R M, Blacklock J R. Finite element analysis of inelastic structures[J]. AIAA Journal, 1969,7:432-438

[20] Raimondo L, Iannucci L, Robinson P, et al. A progressive failure model for mesh-size-independent FE analysis of composite laminates subject to low-velocity impact damage[J]. Composites Science and Technology, 2012, 72(5): 624-632.

[21] Donadon M V, Iannucci L, Falzon B G, et al. A progressive failure model for composite laminates subjected to low velocity impact damage[J]. Computers & Structures, 2008, 86(11): 1232-1252.

[22] Faggiani A, Falzon B G. Predicting low-velocity impact damage on a stiffened composite panel[J]. Composites Part A: Applied Science and Manufacturing, 2010, 41(6): 737-749.

[23] Standard, A. S. T. M. "Standard test methods for shear properties of composite materials by the V-notched beam method." West Conshohocken (PA): ASTM100 (1997).

[24] Turon A, Davila C G, Camanho P P, et al. An engineering solution for mesh size effects in the simulation of delamination using cohesive zone models[J]. Engineering fracture mechanics, 2007, 74(10): 1665-1682.